RSC Advances

PAPER

View Article Online
View Journal | View Issue

Cite this: *RSC Adv.*, 2021, **11**, 7904

Nano BEA zeolite catalysts for the selective catalytic cracking of n-dodecane to light olefins

Galal A. Nasser,[a] M. H. M. Ahmed,[a] Mochamad A. Firdaus,[a] Mohammed A. Sanhoob,[a] Idris A. Bakare,[a] E. N. Al-Shafei,[b] M. Z. Al-Bahar,[b] A. N. Al-Jishi,[b] Z. H. Yamani,[a] Ki-Hyouk Choi[b] and Oki Muraza *[a]

Received 15th September 2020
Accepted 5th January 2021

DOI: 10.1039/d0ra07899a

rsc.li/rsc-advances

Nano BEA zeolite catalysts were synthesized and modified by desilication and then ion-exchanged with Co. The desilication was carried out using 0.1 M of NaOH. The synthesized and modified nano BEA catalysts were characterized *via* different characterization techniques. Ammonia temperature program desorption (NH_3-TPD) and the pyridine Fourier transform infrared (pyridine-FTIR) were utilized to investigate the acidity of catalysts. X-ray diffraction (XRD), ^{27}Al and ^{29}Si nuclear magnetic resonance (NMR) spectroscopy techniques were used to examine the structure of the catalysts. The XRD patterns of the as-synthesized nano BEA catalysts were identical to that of the reference, while the NMR analysis revealed the distribution of silicon and aluminum in the BEA structure. The scanning electron microscope (SEM) analysis confirmed that the fabricated catalysts were less than 100 nm. The desilication and Co ion-exchange altered the acidity of the catalyst. The catalysts were evaluated in the cracking of sssssss to light olefins in the temperature range from 400 °C to 600 °C. The conversion increased with the increase in the reaction temperature for both catalysts; the conversion was above 90% for the Co-BEA catalyst at a temperature above 450 °C. The yield of light olefins also increased at higher temperatures for both catalysts, while at a lower temperature the yield to light olefins was *ca.* 40% over that of Co-BEA.

1.0 Introduction

Light olefins are of high importance as an intermediate feedstock for the petrochemical industries. The demand for these valuable chemicals has been increasing over years. Several raw materials have been converted to olefins beside other products; vacuum gas oil (VGO) has been used as a feedstock in the well-known FCC process, which is the most dominant technology for olefin production.[1,2] Light and heavy naphtha hydrocarbons have also been investigated and different feeds such as *n*-hexane,[3–6] *n*-heptane[7] and n-dodecane[8,9] were studied. Normal dodecane (n-dodecane) with 12 carbon atoms (C_{12}) is an essential building block sourced from both bio and fossil fuels.[10,11] The availability of different and sustainable sources of n-dodecane has garnered considerable attention for its conversion to valuable chemicals with the aid of zeolite catalysts.

Zeolites are crucial solid catalysts that have been utilized in several types of reactions such as cracking,[5,12–18] isomerization,[19–21] alkylation,[22] combustion, cross-coupling,[23] oligomerization,[24] and more.[25–31] Numerous zeolitic materials have been proven to have superior activity in the cracking reaction.[2,6,9,12,15,32–39] Among those is the BEA zeolite, which has a 12-member ring with a pore size of up to 0.7 nm. The BEA zeolite is built by a network of silica and alumina tetrahedra to form a three-dimensional pore system.[34,40] The synthesis of the BEA zeolite framework might involve the use of organic structure-directing agents (OSDAs) or in the absence of OSDA, which is known as the OSDA-free synthesis. The potential advantage of OSDA is that it works as a template in which silica and alumina tetrahedra are formed on to generate a specific structure. The OSDAs or templates aid the fabrication of zeolites with high and tunable Si/Al ratios.[41] Tetraethylammonium hydroxide (TEAOH) is an example of the most commonly used OSDA for the synthesis of a beta zeolite structure. As for the OSDA-free synthesis route, the downside is the inability to synthesize beta (BEA) zeolites with a high Si/Al ratio.

A BEA zeolite has been synthesized with different recipes under static conditions with the reaction temperature in the range of 150–170 °C and crystallization time of up to 96 h.[39,42–44] Also, post-modification techniques have been employed to change the BEA catalyst surface to maximize the product yield of the catalytic cracking reaction. The post-modification techniques that have been used include desilication,[38,44–46] dealumination,[6,15,44,47–50] or the combination of both, followed by ion-exchange with several metals.[16,44] The desilication process is done to create mesoporosity by removing silica using an alkaline solution such as sodium hydroxide (NaOH) or potassium

[a]*Center of Excellence in Nanotechnology and Chemical Engineering Department, King Fahd University of Petroleum and Minerals, Dhahran 31261, Saudi Arabia*
[b]*Research and Development Center, Saudi Aramco, Dhahran 31311, Saudi Arabia. E-mail: omuraza@kfupm.edu.sa*

hydroxide (KOH), whereas dealumination is carried out to strip alumina from the zeolite crystal framework using an acid solution such as nitric acid.[34,44,45,49]

Sanhoob *et al.*[51] post-modified a commercial BEA zeolite by desilication using different agents and applied it in the catalytic cracking of n-dodecane. The applied post-modifications enhanced the n-dodecane conversion from 29% to 76%. Hassan *et al.*[8] studied the performance of parent and modified BEA zeolites. The modification of the BEA zeolite was achieved by desilication to make mesoporosity, and then they incorporated Ni, Co, and a combination of both. The incorporation of Ni and Co affected the acidity of the catalyst; Ni incorporation increased both moderate and strong acid sites to some extent. Furthermore, they observed that the loading of Co into the BEA zeolite caused a further increase in the acid sites, while the combination of both types of metals resulted in the highest acidity. The conversion of n-dodecane on the parent BEA at 400 °C was 22% and it dropped to 3% at TOS of 3 h. The quick deactivation of the parent BEA could be explained by the action of Brønsted acid that facilitated cracking to form paraffins. After the desilication process, the amount of Brønsted acid sites decreased, while the amount of Lewis acid increased. Thus, the conversion dropped to 11%. Moreover, M. Hassan *et al.*[44] synthesized BEA zeolites with different Si/Al ratios: 6, 12.5, 25, 50, and 100. The synthesized BEA catalysts were modified by desilication, dealumination and then ion-exchanged with zirconium. The catalysts were evaluated in the conversion of n-dodecane at 350 °C in the presence of steam. The BEA catalyst with a Si/Al ratio of 25 performed the best and converted around 45 wt% of the feed. Furthermore, other researchers have investigated the effect of the silane content on the BEA zeolite surface to prevent dealumination during the steam-assisted catalytic cracking reaction.[37,39,48,52] Another effort to enhance beta zeolite characteristics was made by converting the crystals into nanoscale units.[9,15,32,37,39,44,53]

Herein, we report the synthesis of the nano BEA zeolite (BEA-P) and modifications of BEA-P by desilication and then ion-exchange with Co (BEA-Co). The developed nano BEA catalysts were evaluated in the conversion of n-dodecane to light olefins at different reaction temperatures. We performed several characterization techniques to understand the properties of the as-prepared nanocatalysts.

2.0 Experimental

2.1. Materials and chemicals

Colloidal silica ST-40 (Nissan chemicals, lot no. 240426), TEAOH (40% aqueous solution), sodium aluminate ($NaAlO_2$), RO water, surfactant (O-15), and sodium hydroxide (NaOH).

2.2. Catalysts synthesis

The nano BEA zeolite (named BEA-P) was synthesized by mixing colloidal silica, water and TEAH. Next, the required amount of sodium aluminate was added to the solution and stirred vigorously for 1 h before transferring it to the surfactant solution. For the synthesis of 50 g of the final gel, 21.1 g of colloidal silica was dissolved in 9.7 g of deionized water, followed by the addition of 18.2 g of TEAOH. After stirring the previous solution for 10 min, 0.92 g of sodium aluminate was added, and the solution was aged for 1 h under stirring. In another synthesis bottle, the O-15 surfactant solution was prepared by melting *ca.* 120 g of O-15 at 55 °C in isopropanol. To the surfactant solution, the final gel of nano BEA-P was added slowly and stirred for 1 h. The final gel was transferred into a teflon-sealed autoclave and crystallized at 150 °C for 3 days. After crystallization, the hydrothermally treated sample was cooled down to room temperature and separated using a centrifuge. The sample was washed several times using distilled water till the pH was around 7. Moreover, the as-synthesized BEA zeolite was dried at 100 °C overnight and then calcined at 550 °C in air for 4–6 h.

2.3. Catalysts post modification

The as-synthesized BEA zeolite (BEA-P) catalyst was modified by the desilication process: 1 g of BEA-P was mixed with 30 ml of 0.1 M NaOH and stirred for 15 min at 65 °C. Then, the catalyst was separated by centrifugation and then ion-exchanged with 0.2 M $CoNO_3$ under the same experimental conditions as those followed for the desilication procedure. Finally, the sample was protonated by ion-exchange with 2 M of ammonium nitrate and calcined at 550 °C for 6 h.

2.4. Characterization techniques

2.4.1. Structure characterization. The structures of BEA-P and BEA-Co were studied *via* X-ray diffraction (XRD) and ^{27}Al, and ^{29}Si nuclear magnetic resonance (NMR) spectroscopy techniques. XRD was recorded using a Rigaku Miniflex diffractometer that was equipped with Cu Kα. The XRD patterns were recorded in the 2θ range of 5–50°, step size of 0.02°, and a scan speed of 3° per min. A 4 mm probe was used in the spectrometer to obtain the ^{29}Si and ^{27}Al NMR spectra using a 30° pulse in a single experiment. The sampling frequencies for ^{29}Si and ^{27}Al spectra were 10 kHz and 113 kHz, respectively. For the ^{29}Si spectrum, the acquisition time of 50 milliseconds was used and a total of 640 scans were accumulated, while for the ^{27}Al spectrum a total of 2000 scans were accumulated for each spectrum.

2.4.2. Morphology and physical property characterizations. Field-emission scanning electron microscopy (FE-SEM) and energy dispersive X-ray spectroscopy (EDS) techniques were used to study morphology and elemental analysis, respectively, of the as-synthesized catalysts. The acidity of BEA-P and BEA-Co catalysts was evaluated using ammonia temperature-programmed desorption (NH_3–TPD) and pyridine Fourier transform infrared (pyridine-FTIR) techniques. NH_3-TPD is commonly used to identify and quantify weak and strong acid sites. The weak acid sites can be identified by the desorption of ammonia at a lower temperature, while strong acid sites are identified by the desorption of ammonia at a higher temperature. The analysis of NH_3-TPD was conducted using a Chemisorb 2750 Micrometric Chemisorption analyzer. First, 0.1 g of the catalyst was heated to 600 °C at 30 °C per min and dwelled for 30 min. After that, the sample was cooled to 100 °C and diluted ammonia was flushed over the catalyst at a flow rate of

30 mL h^{-1} for 30 min. Next, helium was purged to remove the weakly adsorbed ammonia. Then, the catalyst was heated to 700 °C at a heating rate of 10 °C per min, and the desorbed ammonia was detected using a TCD detector. By using the same machine, the hydrogen temperature programm reduction (H_2-TPR) was utilized to study the reducibility of the BEA-Co catalyst. A 50 mg of the catalyst was treated with 30 mL h^{-1} of Ar at 200 °C for 2 h. Right after, the sample was cooled to 50 °C and a gas mixture (10% H_2 in Ar) was allowed to flow over the sample. Then, the temperature was ramped to 800 °C at a heating rate of 10 °C per min and consumption of H_2 was measured.

However, the NH_3-TPD technique was unable to distinguish between Brønsted acid sites and the Lewis acid sites. Thus, pyridine-FTIR has been used to determine and quantify the Brønsted and Lewis acid sites. The analysis was performed using a Nicolet-6700 spectrometer; first, 30 mg of the catalyst was pressed in the form of a wafer that was placed inside a ZnSe IR cell. Following this, the catalyst in the form of a wafer was treated at 500 °C for 30 min and then cooled to 150 °C. The RI spectrum was recorded prior to the pyridine adsorption at 150 °C. Subsequently, the catalyst was saturated with pyridine vapor at 200 Pa for 15 min, and the cell was evacuated to remove the weakly adsorbed pyridine. Thereafter, the IR spectrum was recorded at 150 °C. The IR spectrum before pyridine adsorption was subtracted from IR after pyridine saturation. The Brønsted acid sites were recognized by the appearance of a peak in the IR spectrum at *ca.* 1545 cm^{-1}, while the Lewis acid sites were identified by the presence of a peak at 1450 cm^{-1}. The concentrations of the acid sites were calculated using the following equation:

$$C = A\varepsilon xSm$$

where C is the concentration of acid sites (mmol g^{-1}), A is the area under the peak in the IR spectrum (cm^{-1}), ε is the coefficient and it takes the value of 1.13 cm mol^{-1} for Brønsted acid and 1.28 cm mol^{-1} for Lewis acid. For the normal FTIR measurement, 2 wt% of zeolite was mixed with KBr and then the FTIR measrument was performed over a 30 mg of the composite in the form of a wafer.

The reducibility of cobalt in the BEA zeolite structure was evaluated using a MicrotracBEL (BellCatII) chemisorption equipment. A 300 mg of the sample was placed in the middle of a quartz tube and quartz wool was used to hold the catalyst. The catalyst was first treated at 200 °C for 1 h under the flow of Ar and then cooled to 50 °C. Subsequently, the temperature was ramped to 700 °C under the flow of H_2 and Ar at 50 cm^3 min^{-1}. The hydrogen uptake was measured using a thermal conductivity detector (TDC).

2.4.3. Catalytic cracking of n-dodecane. The catalytic activity of BEA-P and BEA-Co catalysts were conducted in a fixed-bed reactor with an internal diameter of 8 mm at different reaction temperatures. A 1.5 cm^3 catalyst was loaded at the middle of the reactor between quartz wool. The n-dodecane feed flow was set at the liquid hourly space velocity (LHSV) of 10 h^{-1}, using nitrogen gas as a carrier gas at a flow rate of 30 mL min^{-1}. The gaseous effluents from the reactor were separated and sent online to a GC for the product analysis (Fig. 1). The conversion and yield were calculated using the following equations:

$$\text{Conversion} = \frac{\text{concentration } C_{12} \text{ of in the products}}{\text{concentration of } C_{12} \text{ in the feed}} \times 100$$

$$\text{Yield}_i = \frac{[C_i] \text{ in the products}}{\text{Total concentration of products}} \times 100$$

3.0 Results and discussion

3.1. Structure of nano BEA catalysts

The structure of the parent and modified BEA zeolite catalysts were investigated using XRD and NMR techniques. Fig. 2 shows the XRD patterns of the parent (BEA-P) and modified BEA zeolite catalysts with cobalt (BEA-Co). It is obvious that the parent BEA zeolite catalyst shows the typical XRD pattern of the BEA zeolite. The modification of BEA-P by desilication and then by the ion-exchange with Co did not change the catalyst structure; all the peaks of the XRD patterns were retained after the modification. Fig. 3 shows normal FTIR spectra for parent and cobalt-modified BEA zeolite catalysts. Although the spectra appeared to be the same, focusing on the wavenumber region from 400 to 700 cm^{-1}, the transmittance bands at 424, 475, 677 cm^{-1} corresponding to Co–O bonds were observed. The elemental analysis presented in Table 1 revealed the successful incorporation of cobalt into the BEA zeolite structure. The

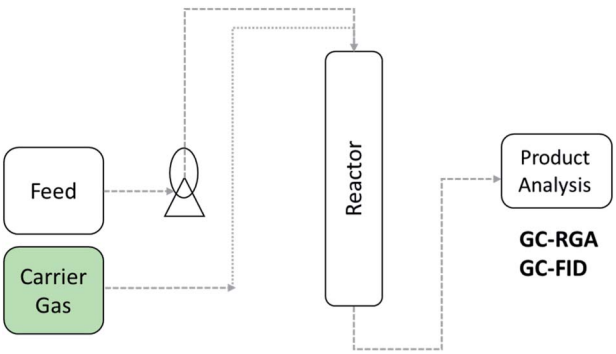

Fig. 1 Experimental setup.

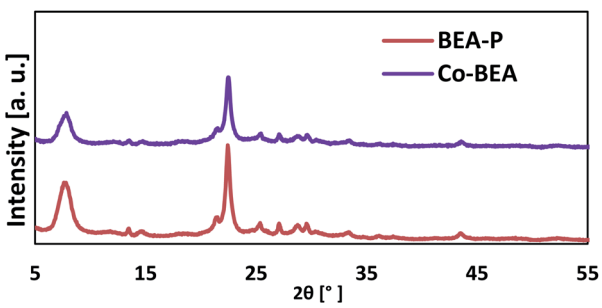

Fig. 2 XRD patterns of parent nano BEA and modified nano BEA zeolite catalysts.

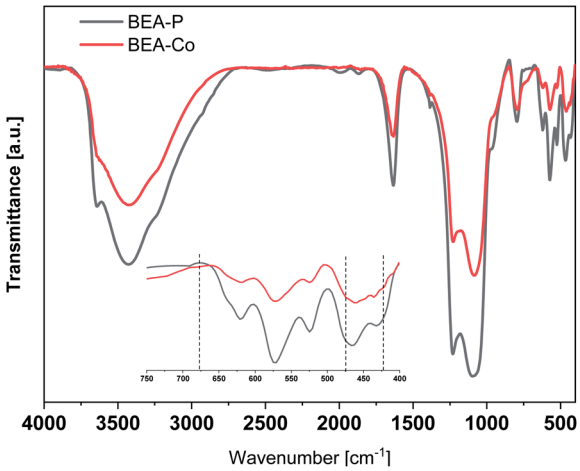

Fig. 3 FTIR spectra of parent BEA and BEA zeolite modified with cobalt.

analysis supports the NMR results, which indicated that the Al atoms were still in the framework and were not severely affected by the desilication process. The light removal of Si was obvious by the decline in the Si/Al ratio from 18.94 to 15.51.

The ^{29}Si and ^{27}Al NMR are potential techniques used to explore the coordination system of Si and Al NMR in the zeolite framework. Basically, silicon is attached to four oxygen atoms to form a tetrahedral coordination (SiO_4).[54] The silicon tetrahedral coordination can have five different coordination systems that correspond to the appearance of five peaks at different chemical shifts in the NMR spectrum.[54–56] Most often, the five SiO_4 coordination systems may appear when the Si/Al ratio is not higher than 10.[54] Fig. 4 shows the ^{27}Al and ^{29}Si NMR spectra of BEA-P and BEA-Co catalysts. The two catalysts exhibited the presence of tetrahedral coordination of Al at a chemical shift of *ca.* 55 ppm and octahedral coordination at a chemical shift of around 0 ppm. However, the peak intensity and the ratio of the tetrahedral area under the peak to that of the octahedral is higher for parent catalyst than that of the BEA-Co catalyst. This indicates that the application of mild desilication and then ion-exchange with cobalt partially removed the extra framework of alumina. However, having a higher peak intensity is related to higher population of the framework type in the zeolite structure.[56] Similarly, the ^{29}Si NMR spectrum showed a difference in peak intensities between the BEA-P and BEA-Co catalysts. The spectrum revealed the presence of the Q^4, Q^3 and Q^2 coordination systems of silicon in the zeolite framework.[54]

Table 1 Elemental analysis of parent and modified BEA zeolites with cobalt by EDS

	Weight%	
Element	BEA-P	BEA-Co
Si	43.57	27.60
Al	2.30	1.78
O	54.13	69.76
Co	—	0.86
Total	100.00	100.00
Si/Al	18.94	15.51

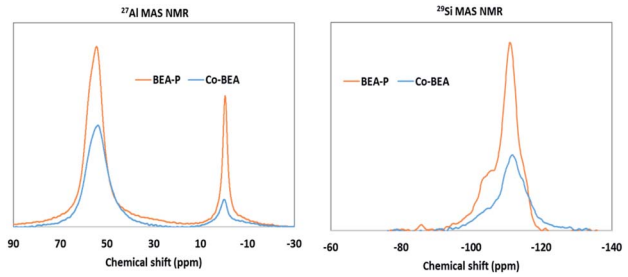

Fig. 4 ^{27}Al MAS and ^{29}Si MAS NMR of parent nano BEA (BEA-P) and modified nano BEA (BEA-Co).

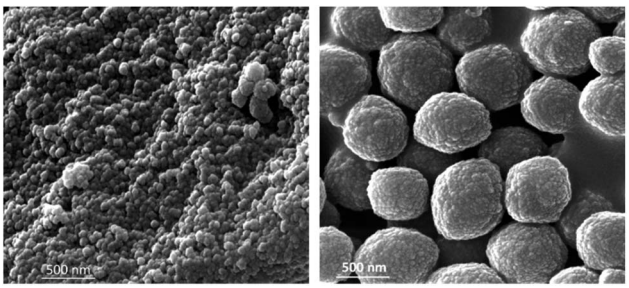

Fig. 5 FE-SEM images of nano and submicron BEA zeolite.

3.2. Morphology and physical properties of nano BEA catalysts

The FE-SEM images of the nano BEA zeolite catalyst synthesized using the emulsion method, and the submicron BEA zeolite catalyst prepared without the presence of the surfactant are presented in Fig. 5. It is obvious that the synthesis of the BEA zeolite by the emulsion method has reduced the particle size from ~500 nm when the surfactant was not used to less than 100 nm. T *et al.* reported the role of a surfactant in general and O-15 in particular on the size and particle morphology of a zeolite.[57] The specific role of a surfactant is to increase the nucleation rate of zeolite crystals by adsorption on solid surfaces in the solution.

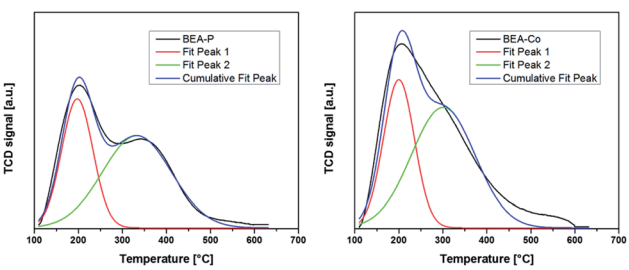

Fig. 6 Ammonia-TPD profile of parent nano BEA and modified nano BEA-Co.

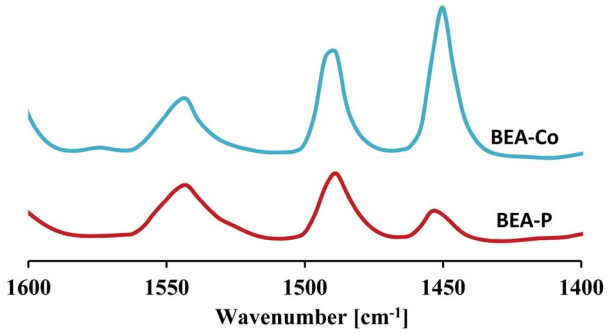

Fig. 7 Pyridine FTIR profile of parent BEA and modified BEA.

3.4. Acidity of nano BEA zeolite catalysts and reducibility of BEA-Co

In one method, the acidity of nano BEA catalysts was investigated by the detection of ammonia desorbed from the catalysts as the temperature was increased. The NH_3-TPD profiles presented in Fig. 6 reveal the presence of a low-temperature peak (LTP) centered at *ca.* 200 °C attributed to weak acid sites. Both catalysts exhibited the same LTP but with a relatively higher intensity for the BEA-Co catalyst. Another medium temperature peak (MTP) observed at around 350 °C was ascribed to medium acid sites. MTP was obvious in parent nano BEA catalysts, while in BEA-Co catalysts, it overlapped with LTP. Thus, we conducted a Gaussian deconvolution to separate the two peaks, as shown in Fig. 6. The increase in the amount of acidity for the BEA-Co catalyst is due to the formation of CoO_4^{2-} tetrahedra in mesoporous structures.[8,58]

In another method, we used pyridine-FTIR to distinguish Bronsted acid sites from Lewis acid sites. From Fig. 7 and Table 2, it can be seen that the nano parent BEA catalyst exhibited a relatively higher amount of Brønsted acidity and a low amount of Lewis acidity. The desilication of the nano BEA catalyst and then ion-exchange with Co caused a noticeable increase in the amount of Lewis acid sites and a slight decrease in Brønsted acid sites. The Lewis acid sites are related to the appearance of the extra aluminum in the framework of the zeolite structure.[38] In our case, the extra framework might be because of the consequence of desilication and ion-exchange procedures.

The temperature program reduction of hydrogen (H_2-TPR) profiles are shown in Fig. 8. The hydrogen consumption is represented by different peaks at different temperatures. The hydrogen uptake at a lower temperature is assigned to the reduction of Co_3O_4, while consumption at a higher temperature is attributed to what is known as the "spinel-like phase".[59,60] The peaks at *ca.* 350 °C and 400 °C are ascribed to the reduction of Co^{3+} to Co^{2+} and Co^{2+} to Co, respectively.

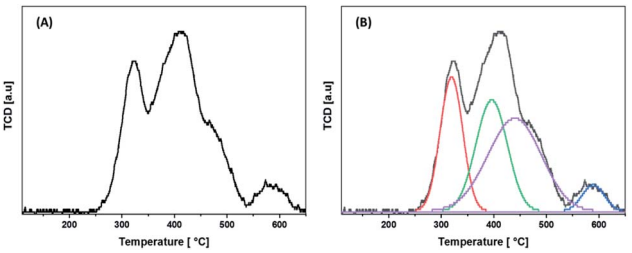

Fig. 8 H_2-TPR profile of BEA-Co; original hydrogen uptake (A) and deconvoluted hydrogen uptake (B).

3.5. Catalytic evaluation of nano BEA catalysts

The conversions of n-dodecane (C_{12}) over parent nano BEA (BEA-P) and nano BEA modified with Co (BEA-Co) zeolite catalysts as a function of temperature are shown in Fig. 9. At lower temperatures, BEA-Co showed a higher conversion than that by the parent catalyst BEA-P. Initially, when the temperature was 400 °C, BEA-P converted *ca.* 75% of C_{12}, while BEA-Co achieved a conversion of around 89%. An increase in temperature to 450 °C caused a noticeable enhancement of the conversion, particularly for BEA-P. The conversion over BEA-P was enhanced by 16.5% to reach *ca.* 92%, while that on BEA-Co increased by 9% and reached *ca.* 98%. Both catalysts exhibited a similar C_{12} conversion with a further increase in the reaction temperature

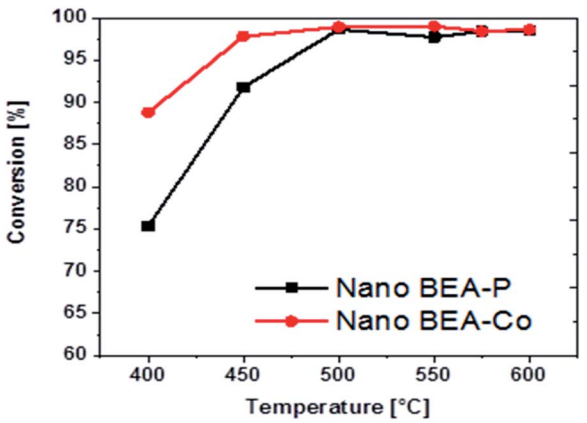

Fig. 9 Conversion of n-dodecane over nanoparent BEA (BEA-P) and nano-modified BEA with Co (BEA-Co) at different reaction temperatures.

Table 2 Brønsted and Lewis acid density derived from the adsorption of pyridine over parent and modified BEA zeolite

Sample	T (°C)	Weight (mg)	CL (mmol g^{-1})	CB (mmol g^{-1})	Total acidity	L/B
BEA-P	150	30.00	0.091	0.352	0.433	0.258
BEA-Co	150	30.00	0.282	0.194	0.475	1.454

Table 3 Products distribution of cracking of n-dodecane over nano BEA-P catalyst at different reaction temperatures

	Temperature [°C]					
Product [%]	400	450	500	550	575	600
Gas yield	67	86	97.3	97.3	98.1	97.7
Conversion	75.3	91.8	98.6	97.7	98.4	98.5
Total olefins	26.8	34.2	44.4	51.4	58.3	61.2
P/E	—	19.3	10.1	3.7	2	1.1
Dry gas	24.9	26.1	32.7	31.7	26.1	25.5
Butenes	16.2	18.9	21.6	18.7	20.3	17.4
Ethylene	0	0.8	2.1	7	12.8	21.2
Propylene	10.7	14.5	20.8	25.7	25.2	22.6
H_2	0.1	0.3	2.7	6.4	6.9	7.2
Methane	0	0	0.7	3.3	7.2	12.6
C_2	0.3	0.3	0.4	2	3.9	6

up to 600 °C, as presented in Tables 3 and 4. The high activity of the BEA-Co catalyst at a lower temperature might be related to the density of Brønsted and Lewis acid sites. Even though both catalysts possess almost the same amount of total acidity, the ratio of the Lewis to Brønsted (L/B) acid is higher in the modified catalyst BEA-Co. Under similar reaction conditions, the performance of the fabricated nano BEA zeolite catalysts in the cracking of heavy hydrocarbons is superior compared with different types of BEA zeolite catalysts, as reported in the literature.[8,38,44,51] Tarach *et al.*[38] desilicated a BEA zeolite catalyst and then evaluated the catalyst in the cracking of *n*-decane. The catalytic cracking of the BEA zeolite at different catalyst to oil ratios and at a reaction temperature of 500 °C indicated convertions from *ca.* 65–82% for the decane fed into the reactor. Sanhoob *et al.*[51] tested parent and modified commercial BEA zeolites in the cracking of n-dodecane in the presence of 10% steam at 350 °C. The BEA catalyst showed a conversion of n-dodecane of only 30 wt%.

Fig. 10 shows the percentage of gas and olefin (C_2–C_4) yield at different reaction temperatures for the parent nano BEA and modified BEA-Co catalysts. The trend of the gas yield was

Table 4 Products distribution of cracking of n-dodecane over nano BEA-Co catalyst at different reaction temperatures

	Temperature [°C]					
Products [%]	400	450	500	550	575	600
Gas yield	85.7	95.2	96.3	96.7	97.2	97.6
Conversion	88.8	97.8	98.9	99	98.4	98.6
Total olefins	40	46.4	45.7	47.7	52.1	53.8
P/E	24.1	11.7	3	1.6	0.6	0.5
Dry gas	31.4	29.9	27.1	25.1	25.2	26.5
Butenes	24.9	24.5	15.9	13.2	11.3	7.9
Ethylene	0.6	1.7	7.5	13.3	24.9	31.4
Propylene	14.4	20.1	22.4	21.3	15.9	14.4
H_2	1.9	6.6	12.9	17.5	16.5	14.6
Methane	0	0.7	4.3	8.8	15	17.8
C_2	0.2	0.6	2.6	4.8	7.7	7.3

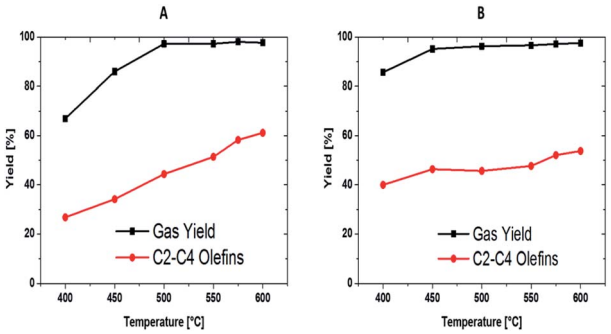

Fig. 10 Percent of gas produced, and olefins yield over parent nano BEA (A) and nano BEA modified with Co (B).

similar to the trend of the overall conversion as most of the liquid produced was mainly C_{12}. The gas yields at 400 °C were *ca.* 67% and 86% for BEA-P and BEA-Co, respectively. Then, the yield increased to 86% over BEA-P and up to 95% over the BEA-Co catalyst at a temperature of 450 °C. At elevated reaction temperatures, the gas yield was more than 96% for all catalysts.

The two catalysts showed good olefin yield, as presented in Fig. 10, Tables 3 and 4. The olefin yield of BEA-P was *ca.* 27%, which then increased to 34% when the temperature was raised from 400 °C to 450 °C, while BEA-Co showed better olefin yields of 40% and 46% at the same reaction temperatures. At 500 °C, all catalysts almost showed the same amount of olefins produced. However, by further increasing the reaction temperature from 550 °C up to 600 °C, interestingly BEA-P proved to be more selective towards olefins, in which the yield was *ca.* 61% over BEA-P and *ca.* 54% over BEA-Co. Thus, Fig. 11 is presented to pay special attention to the selectivity of each olefin. All species behaved differently over the two catalysts at different reaction temperatures. For example, butene yield over BEA-P was *ca.* 16% at 400 °C, which then increased with the increase

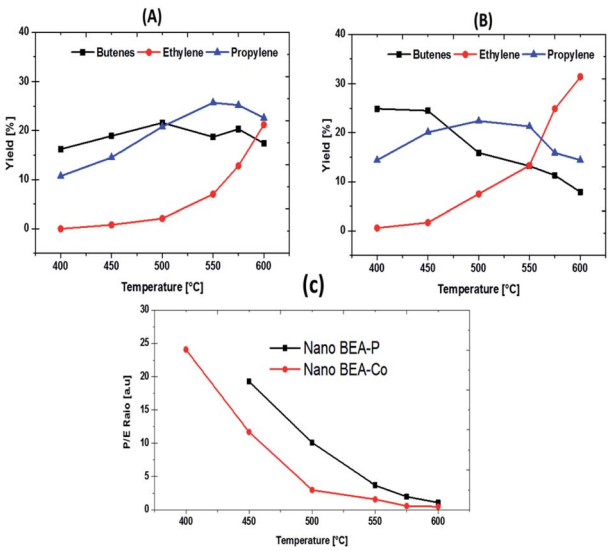

Fig. 11 C_2–C_4 olefins yield over parent BEA (A) and BEA modified Co (B) catalysts and propylene to ethylene ratio of both catalysts as a function of temperature (C).

in reaction temperature up to 22% at 500 °C. A further upsurge in temperature to 600 °C reduced the yield of butenes to around 17%. In contrast, the BEA-Co catalyst produced a higher amount of butenes, *ca.* 25%, at lower reaction temperatures and then it decreased with the increase in reaction temperature to around 8% at 600 °C. This suggests that butenes were converted to lower hydrocarbons on BEA-Co as the reaction temperature increased. The propylene yield curve over BEA-Co is like a parabola that is open down at both ends at high and low temperatures; the maximum yield was *ca.* 22% at 500 °C. For the BEA-P catalyst, the propylene yield increased along with temperature and reached a maximum of *ca.* 25% at 575 °C and then was started to decline when the temperature was 600 °C. Furthermore, the amount of ethylene produced over both catalysts increased with the increase in the reaction temperature. Though it is worth mentioning that BEA-Co showed higher ethylene selectivity at the different reaction temperatures (please see Tables 2 and 3). In addition, the nano BEA catalyst modified with Co enhanced the olefin selectivity at lower temperatures.

4.0 Conclusions

In conclusion, a nano BEA zeolite in the size range of 50–100 nm was successfully synthesized and modified by Co. Both catalysts presented superior activity in the cracking of n-dodecane to lower and more valuable hydrocarbons. However, nano-BEA-Co presented better activity and selectivity at lower temperatures and thus showed low energy consumption with better olefin production.

Conflicts of interest

There are no conflicts to declare.

Acknowledgements

The authors would like to acknowledge the funding provided by Saudi Aramco for Center of Research Excellence in Nanotechnology at King Fahd University of Petroleum & Minerals (KFUPM).

References

1 A. A. Al-Absi and S. S. Al-Khattaf, Conversion of Arabian light crude oil to light olefins via catalytic and thermal cracking, *Energy and Fuels*, 2018, **32**, 8705–8714.
2 R. Imai, T. Takatsuka, K. Maeda, A. Fukazawa, N. Takahashi and H. Fukunaga, Multidimensional Reaction Control with Beta Type Zeolites in Heavy Oil Catalytic Cracking, *J. Jpn. Petrol. Inst.*, 2013, **56**, 317–325.
3 J. Abbot and B. W. Wojciechowski, Catalytic Reactions of Normal-Hexane on Hy Zeolite, *Can. J. Chem. Eng.*, 1988, **66**, 825–830.
4 Y. Nakasaka, T. Okamura, H. Konno, T. Tago and T. Masuda, Crystal size of MFI-type zeolites for catalytic cracking of n-hexane under reaction-control conditions, *Microporous Mesoporous Mater.*, 2013, **182**, 244–249.
5 H. E. van der Bij, F. Meirer, S. Kalirai, J. Wang and B. M. Weckhuysen, Hexane Cracking over Steamed Phosphated Zeolite H-ZSM-5: Promotional Effect on Catalyst Performance and Stability, *Chem.–Eur. J.*, 2014, **20**, 16922–16932.
6 A. Yamaguchi, D. F. Jin, T. Ikeda, K. Sato, N. Hiyoshi and T. Hanaoka, Effect of steam during catalytic cracking of n-hexane using P-ZSM-5 catalyst, *Catal. Commun.*, 2015, **69**, 20–24.
7 A. Corma, V. Fornes, F. V. Melo, J. B. Monton and A. V. Orchilles, Catalytic Cracking of a Vacuum Gas-Oil and N-Heptane on H-Beta Zeolites with Different Si/A1 Ratios, *Abstr. Pap. Am. Chem. Soc.*, 1987, **194**, 14.
8 M. H. M. Ahmed, O. Muraza, A. K. Jamil, E. N. Shafei, Z. H. Yamani and K. H. Choi, Steam Catalytic Cracking of n-Dodecane over Ni and Ni/Co Bimetallic Catalyst Supported on Hierarchical BEA Zeolite, *Energy Fuels*, 2017, **31**, 5482–5490, DOI: 10.1021/acs.energyfuels.7b00468.
9 A. Ishihara, K. Inui, T. Hashimoto and H. Nasu, Preparation of hierarchical beta and Y zeolite-containing mesoporous silica-aluminas and their properties for catalytic cracking of n-dodecane, *J. Catal.*, 2012, **295**, 81–90.
10 T. Imam and S. Capareda, Characterization of bio-oil, syn-gas and bio-char from switchgrass pyrolysis at various temperatures, *J. Anal. Appl. Pyrolysis.*, 2012, **93**, 170–177.
11 Y. Shi, E. Xing, K. Wu, J. Wang, M. Yang and Y. Wu, Catalysis Science & Technology MINIREVIEW Recent progress on upgrading of bio-oil to hydrocarbons over metal/zeolite bifunctional catalysts, *Catal.: Sci. Technol.*, 2017, **7**, 2385, DOI: 10.1039/c7cy00574a.
12 T. Sonthisawate, T. Nakanishi, H. Nasu, T. Hashimoto and A. Ishihara, Catalytic cracking reaction of vacuum gas oil and atmospheric residue by zeolite-containing microporous and mesoporous composites using Curie point pyrolyzer, *Fuel Process. Technol.*, 2016, **142**, 337–344.
13 D. Karami and N. Mahinpey, Application of Novel Zeolite Y Nanoparticles in Catalytic Cracking Reactions, *Chem. Eng. Commun.*, 2015, **203**, 251–257.
14 A. A. Al-Absi, A. M. Aitani and S. S. Al-Khattaf, Thermal and catalytic cracking of whole crude oils at high severity, *J. Anal. Appl. Pyrolysis*, 2020, **145**, 104705.
15 W. N. Wang, W. Zhang, Y. L. Chen, X. D. Wen, H. Li and D. L. Yuan, Mild-acid-assisted thermal or hydrothermal dealumination of zeolite beta, its regulation to Al distribution and catalytic cracking performance to hydrocarbons, *J. Catal.*, 2018, **362**, 94–105.
16 I. A. Bakare, O. Muraza, T. Taniguchi, T. Tago, G. Nasser and Z. H. Yamani, Steam-assisted catalytic cracking of n-hexane over La-Modified MTT zeolite for selective propylene production, *J. Anal. Appl. Pyrolysis.*, 2015, **116**, 272–280.
17 A. Yamaguchi, D. Jin, T. Ikeda, K. Sato, N. Hiyoshi, T. Hanaoka, F. Mizukami and M. Shirai, Deactivation of ZSM-5 zeolite during catalytic steam cracking of n-hexane, *Fuel Processing Technology*, 2014, **126**, 343–349.

18 X. Xian, C. Ran, P. Yang, Y. Chu, S. Zhao and L. Dong, Effect of the acidity of HZSM-5/MCM-41 hierarchical zeolite on its catalytic performance in supercritical catalytic cracking of n-dodecane: Experiments and mechanism, *Catal.: Sci. Technol.*, 2018, **8**, 4241–4256, DOI: 10.1039/c8cy00908b.

19 L. V. Piryutko, S. V Lazareva, V. S. Chernyayskii, A. S. Kharitonov and A. S. Noskov, Influence of Topology and Chemical Composition of MTT and MFI Zeolites on Catalytic Properties in the Isomerization Reaction of Ethylene Oxide to Acetaldehyde, *Pet. Chem.*, 2019, **59**, 726–732.

20 P. S. F. Mendes, C. Chizallet, J. Pérez-Pellitero, P. Raybaud, J. M. Silva, M. F. Ribeiro, A. Daudin and C. Bouchy, Interplay of the adsorption of light and heavy paraffins in hydroisomerization over H-beta zeolite, *Catal.: Sci. Technol.*, 2019, **9**, 5368–5382, DOI: 10.1039/c9cy00788a.

21 W. Wang, C. J. Liu and W. Wu, Bifunctional catalysts for the hydroisomerization of: N -alkanes: The effects of metal-acid balance and textural structure, *Catal.: Sci. Technol.*, 2019, **9**, 4162–4187, DOI: 10.1039/c9cy00499h.

22 L. B. Zinner, K. Zinner, M. Ishige and A. S. Araujo, Catalytic Activity of Lanthanide-Doped Y-Zeolite on the Alkylation of Benzene with 1-Dodecene Model Reaction, *J. Alloys Compd.*, 1993, **193**, 65–67.

23 A. J. Raiza, K. Pandian and R. G. Kumar, Biosynthesis of Copper Nanoparticles Supported on Zeolite Y and its Application in Catalytic C-N Cross Coupling Reactions between Amines and Aryl halides, *Chemistryselect*, 2019, **4**, 1964–1970.

24 V. A. Vorobkalo, A. G. Popov, L. I. Rodionova, E. E. Knyazeva and I. I. Ivanova, Influence of MEL Zeolite Synthesis Conditions on the Physicochemical and Catalytic Properties in the Oligomerization Reaction of Butylenes, *Pet. Chem.*, 2018, **58**, 1036–1044.

25 N. Y. Ul'yanova and O. Y. Golubeva, Zeolites Modified with Silver Nanoparticles and Clusters: Synthesis, Characterization, and Catalytic Performance in H-2 and CO Oxidation Reactions, *Glass Phys. Chem.*, 2018, **44**.

26 M. S. Zina, L. Bassalah and A. Ghorbel, Extra-network cations of zeolite Y on the catalytic activity of palladium in the combustion reaction of methane, *Can. J. Chem.*, 2009, **87**, 706–713.

27 C. Yokoyama and M. Misono, Catalytic Reduction of Nitrogen Monoxide by Propene in the Presence of Oxygen over Cerium Ion-Exchanged Zeolites.1. General-Characteristics of the Reaction and Effects of Alkaline-Earth Metal Addition, *Bull. Chem. Soc. Jpn.*, 1994, **67**, 557–562.

28 N. Wijayati, N. Hidayah, S. Mursiti and E. Kusumastuti, Catalytic activity of P2O5-natural zeolite on hydration reaction of turpentine into alpha-terpineol, *IOP Conf. Ser.: Mater. Sci. Eng.*, 2019, **509**, 012093.

29 E. Catizzone, M. Migliori, A. Aloise, R. Lamberti and G. Giordano, Hierarchical Low Si/Al Ratio Ferrierite Zeolite by Sequential Postsynthesis Treatment: Catalytic Assessment in Dehydration Reaction of Methanol, *J. Chemom.*, 2019, 3084356.

30 L. T. Bu, K. Orton, K. Iisa, C. Mukarakate and S. Kim, Understanding dehydration reaction and diffusion during biomass catalytic upgrading over ZSM-5 zeolite, *Abstr. Pap. Am. Chem. Soc.*, 2019, **257**, 20036.

31 S. Wang, S. Guo, Y. Luo, Z. Qin, Y. Chen, M. Dong, J. Li, W. Fan and J. Wang, Direct synthesis of acetic acid from carbon dioxide and methane over Cu-modulated BEA, MFI, MOR and TON zeolites: A density functional theory study, *Catal.: Sci. Technol.*, 2019, **9**, 6613–6626, DOI: 10.1039/c9cy01803d.

32 N. Taufiqurrahmi, A. R. Mohamed and S. Bhatia, Deactivation and coke combustion studies of nanocrystalline zeolite beta in catalytic cracking of used palm oil, *Chem. Eng. J.*, 2010, **163**, 413–421.

33 S. Kotrel, M. P. Rosynek and J. H. Lunsford, Intrinsic catalytic cracking activity of hexane over H-ZSM-5, H-beta and H-Y zeolites, *J. Phys. Chem. B.*, 1999, **103**, 818–824.

34 A. Corma, V. Fornes, J. B. Monton and A. V. Orchilles, Catalytic Activity of Large-Pore High Si/Al Zeolites - Cracking of Heptane on H-Beta and Dealuminated Hy Zeolites, *J. Catal.*, 1987, **107**, 288–295.

35 H. Konno, R. Ohnaka, J. Nishimura, T. Tago, Y. Nakasaka and T. Masuda, Kinetics of the catalytic cracking of naphtha over ZSM-5 zeolite: effect of reduced crystal size on the reaction of naphthenes, *Catal. Sci. Technol.*, 2014, **4**, 4265–4273.

36 P. G. Smirniotis and E. Ruckenstein, Comparison of the Performance of Zsm-5, Beta-Zeolite, Y, Usy, and Their Composites in the Catalytic Cracking of N-Octane, 2,2,4-Trimethylpentane, and 1-Octene, *Ind. Eng. Chem. Res.*, 1994, **33**, 800–813.

37 V. P. S. Caldeira, A. Peral, M. Linares, A. S. Araujo, R. A. Garcia-Munoz and D. P. Serrano, Properties of hierarchical Beta zeolites prepared from protozeolitic nanounits for the catalytic cracking of high density polyethylene, *Appl. Catal., A*, 2017, **531**, 187–196.

38 K. Tarach, K. Góra-Marek, J. Tekla, K. Brylewska, J. Datka and K. Mlekodaj, Catalytic cracking performance of alkaline-treated zeolite Beta in the terms of acid sites properties and their accessibility, *J. Catal.*, 2014, **312**, 46–57.

39 U. Khalil, O. Muraza, H. Kondoh, G. Watanabe, Y. Nakasaka and A. Al-Amer, Production of Lighter Hydrocarbons by Steam-Assisted Catalytic Cracking of Heavy Oil over Silane-Treated Beta Zeolite, *Energy Fuels*, 2016, **30**, 1304–1309.

40 *Verified Syntheses of Zeolitic Materials*, ed. S. M. NB, Internationl Zeolite Association, 2016.

41 G. A. Nasser, O. Muraza, T. Nishitoba, Z. Malaibari, T. K. Al-Shammari and T. Yokoi, OSDA-free chabazite (CHA) zeolite synthesized in the presence of fluoride for selective methanol-to-olefins, *Microporous Mesoporous Mater.*, 2019, **274**, 277–285, DOI: 10.1016/j.micromeso.2018.07.020.

42 A. Corma, V. Fornes, F. Melo and J. Pérez-Pariente, Zeolite Beta: Structure, Activity, and Selectivity for Catalytic Cracking, *ACS Symp. Ser.*, 1988, **375**, 49–63.

43 Y. Wang, R. Otomo, T. Tatsumi and T. Yokoi, Selective Production of Light Olefins from Catalytic Cracking of n-

Hexane over OSDA-Free Beta Zeolites, *Catal. Surv. Asia.*, 2016, 20.

44 M. H. M. Ahmed, O. Muraza, A. Galadima, A. K. Jamil, E. N. Shafei, Z. H. Yamani and K. H. Choi, Hydrothermal Stabilization of Rich Al-BEA Zeolite by Post-Synthesis Addition of Zr for Steam Catalytic Cracking of n -Dodecane, *Energy Fuels*, 2018, **32**, 5501–5508, DOI: 10.1021/acs.energyfuels.8b00087.

45 Y. Wang, T. Yokoi, S. Namba and T. Tatsumi, Effects of Dealumination and Desilication of Beta Zeolite on Catalytic Performance in n-Hexane Cracking, *Catalysts*, 2016, **6**, 8.

46 M. Hartmann, A. G. Machoke and W. Schwieger, Catalytic test reactions for the evaluation of hierarchical zeolites, *Chem. Soc. Rev.*, 2016, **45**, 3313–3330.

47 A. Yamaguchi, D. F. Jin, T. Ikeda, K. Sato, N. Hiyoshi and T. Hanaoka, Deactivation of ZSM-5 zeolite during catalytic steam cracking of n-hexane, *Fuel Process. Technol.*, 2014, **126**, 343–349.

48 U. Khalil, O. Muraza, H. Kondoh, G. Watanabe, Y. Nakasaka and A. Al-Amer, Robust surface-modified Beta zeolite for selective production of lighter fuels by steam-assisted catalytic cracking from heavy oil, *Fuel*, 2016, **168**, 61–67.

49 Y. Wang, R. Otomo, T. Tatsumi and T. Yokoi, Dealumination of organic structure-directing agent (OSDA) free beta zeolite for enhancing its catalytic performance in n-hexane cracking, *Microporous Mesoporous Mater.*, 2016, **220**, 275–281.

50 K. Na, J. Yoon and G. A. Somorjai, Control of model catalytic conversion reaction over Pt nanoparticle supported mesoporous BEA zeolite catalysts, *Catal. Today*, 2016, **265**, 225–230.

51 M. A. Sanhoob, U. Khalil, E. N. Shafei, K.-H. Choi, T. Yokoi and O. Muraza, Steam cracking of green diesel (C12) to BTX and olefins over silane-treated hierarchical BEA, *Fuel*, 2020, **263**, 116624.

52 J. Sonoda, T. Kamegawa, Y. Kuwahara, K. Mori and H. Yamashita, Hydrophobic Modification of Ti-Containing Zeolite (TS-1) and Their Applications in Liquid-Phase Selective Catalytic Reactions, *Bull. Chem. Soc. Jpn*, 2010, **83**, 5.

53 M. A. Sanhoob, O. Muraza, T. Taniguchi, T. Tago, G. Watanabe and T. Masuda, Steam Catalytic Cracking of n-Hexane over Modified MTW Zeolites Impregnated by Extra-Framework Elements, *Energy Fuels*, 2016, **30**, 9679–9685.

54 L. Mafra, J. A. Vidal-Moya and T. Blasco, Chapter Four - Structural Characterization of Zeolites by Advanced Solid State NMR Spectroscopic Methods, in *Annual Reports on NMR Spectroscopy*, ed. G. A. Webb, Academic Press, 2012, pp. 259–351.

55 C. A. Fyfe, J. M. Thomas, J. Klinowski and G. C. Gobbi, Magic-Angle-Spinning NMR (MAS-NMR) Spectroscopy and the Structure of Zeolites, *Angew. Chem., Int. Ed. Engl.*, 1983, **22**, 259–275, DOI: 10.1002/anie.198302593.

56 J. Klinowski, Solid-state NMR studies of molecular sieve catalysts, *Chem. Rev.*, 1991, **91**, 1459–1479.

57 M. TTaT, *Zeolite Nanocrystals-Synthesis and Applications*, IntechOpen, Nagoya University, Japan, 2010.

58 M. Rutkowska, Z. Piwowarska, E. Micek and L. Chmielarz, Fe-, Cu- and Co-Beta zeolites obtained by mesotemplate-free method. Part I: Synthesis and catalytic activity in N2O decomposition, *Microporous Mesoporous Mater.*, 2015, **209**, 54–65.

59 L. Obalová, K. Pacultová, J. Balabánová, K. Jirátová, Z. Bastl, M. Valášková, Z. Lacný and F. Kovanda, Effect of Mn/Al ratio in Co-Mn-Al mixed oxide catalysts prepared from hydrotalcite-like precursors on catalytic decomposition of N2O, *Catal. Today*, 2007, **119**, 233–238, DOI: 10.1016/j.cattod.2006.08.027.

60 Q. Shen, L. Li, C. He, X. Zhang, Z. Hao and Z. Xu, Cobalt zeolites: Preparation, characterization and catalytic properties for N2O decomposition, *Asia-Pac. J. Chem. Eng.*, 2012, **7**, 502–509, DOI: 10.1002/apj.599.